11-2015

Identification of Native Defects (Vacancies and Antisites) in $CdSiP_2$ Crystals

Eric M. Golden
Air Force Institute of Technology

Nancy C. Giles
Air Force Institute of Technology

Ember S. Maniego [*]
Air Force Institute of Technology

Frank Kenneth Hopkins
Air Force Research Laboratory

Kevin T. Zawilski
BAE Systems

See next page for additional authors

Recommended Citation

Golden, E. M., Giles, N. C., Maniego, E., Hopkins, F. K., Zawilski, K. T., Schunemann, P. G., & Halliburton, L. E. (2015). Identification of native defects (vacancies and antisites) in CdSiP2 crystals. Journal of Applied Physics, 118(18), 185702. https://doi.org/10.1063/1.4935420

Journal of Applied Physics

Identification of native defects (vacancies and antisites) in $CdSiP_2$ crystals

Cite as: J. Appl. Phys. **118**, 185702 (2015); https://doi.org/10.1063/1.4935420
Submitted: 08 September 2015 . Accepted: 28 October 2015 . Published Online: 11 November 2015

E. M. Golden, N. C. Giles, E. Maniego, F. K. Hopkins, K. T. Zawilski, P. G. Schunemann, and L. E. Halliburton

JOURNAL OF APPLIED PHYSICS **118**, 185702 (2015)

Identification of native defects (vacancies and antisites) in $CdSiP_2$ crystals

E. M. Golden,[1] N. C. Giles,[1] E. Maniego,[1] F. K. Hopkins,[2] K. T. Zawilski,[3] P. G. Schunemann,[3] and L. E. Halliburton[4,a)]

[1]*Department of Engineering Physics, Air Force Institute of Technology, Wright-Patterson Air Force Base, Ohio 45433, USA*

[2]*Air Force Research Laboratory, Materials and Manufacturing Directorate, Wright-Patterson Air Force Base, Ohio 45433, USA*

[3]*BAE Systems, Nashua, New Hampshire 03061, USA*

[4]*Department of Physics and Astronomy, West Virginia University, Morgantown, West Virginia 26506, USA*

(Received 8 September 2015; accepted 28 October 2015; published online 11 November 2015)

Electron paramagnetic resonance (EPR) is used to identify four native defects in single crystals of $CdSiP_2$. This nonlinear optical material is used in optical parametric oscillators to generate tunable output in the mid-infrared. The performance of these frequency-conversion devices is limited when infrared absorption bands associated with native defects overlap a pump wavelength. Cadmium, silicon, and phosphorus vacancies and also silicon-on-cadmium antisites are present in the as-grown undoped $CdSiP_2$ crystals. Using near-band-edge 632.8 nm light from a He-Ne laser, a paramagnetic charge state, and thus an EPR spectrum, is formed at liquid-helium temperatures for three of the four defects. The EPR spectrum from the singly ionized silicon vacancy (V_{Si}^{-}) is present without light and has five hyperfine lines due to equal interactions with the four neighboring ^{31}P nuclei. In contrast, the photoinduced EPR spectrum from the singly ionized cadmium vacancy (V_{Cd}^{-}) has a three-line hyperfine pattern due to equal interactions with only two of its four neighboring ^{31}P nuclei. The light-induced spectrum from the singly ionized silicon-on-cadmium antisite (Si_{Cd}^{+}) also has a three-line hyperfine pattern, thus indicating that the unpaired spin interacts primarily with only two ^{31}P neighbors. For the neutral phosphorus vacancy (V_P^0), the unpaired spin is primarily localized on the nearest-neighbor silicon ions and the photoinduced EPR spectrum has no resolved ^{31}P hyperfine interactions. The silicon and cadmium vacancies are acceptors, and the silicon-on-cadmium antisite and the phosphorus vacancy are donors. © *2015 AIP Publishing LLC*.
[http://dx.doi.org/10.1063/1.4935420]

I. INTRODUCTION

Cadmium silicon diphosphide ($CdSiP_2$, or simply CSP) is a versatile nonlinear optical material that has recently been developed for frequency-conversion applications in the infrared.[1,2] This negative uniaxial II-IV-V_2 chalcopyrite semiconductor has a high nonlinear optical coefficient, a significant birefringence, and good thermomechanical properties. CSP has an optical band edge near 2.2 eV (560 nm), and its transparency extends to 9 μm (with multiphonon absorption peaks starting near 6.6 μm). The electronic structure[3,4] and phase-matching properties[5,6] of CSP have been established. Also, advances in the growth of CSP crystals have been reported.[1,7–10] A series of recent studies have explored the feasibility of using CSP as an optical parametric oscillator (OPO) to generate mid-infrared laser light.[2,11–23] A distinct advantage of CSP, when compared to other available nonlinear optical materials such as $ZnGeP_2$, is its operation as an OPO with pump wavelengths between 1 and 2 μm (e.g., pumping at 1.55 μm yields continuous tunability from 1.7 to 9 μm, and pumping at the highly desirable 1.064 μm wavelength produces output near 6 μm).[1]

The performance of a CSP-based OPO will be degraded if one or more broad absorption bands are present in the pump region. (The maximum output power may be reduced and emerging beams may be distorted.) Native point defects (vacancies and antisites) introduced during growth of the crystals are often responsible for these device-limiting absorption bands.[24–26] Electron paramagnetic resonance (EPR), with its high resolution and high sensitivity, is an experimental technique[27,28] well-suited to identify native defects (donors and acceptors) in these CSP crystals through the study of their paramagnetic charge states. Depending on the degree of compensation and the position of the Fermi level within the material's energy gap, many of the point defects in a CSP crystal do not initially have an unpaired spin. These defects can be temporarily converted into a metastable EPR-active charge state by redistributing electrons within the crystal during an exposure to the appropriate wavelength of laser light while the sample is held at low temperature.

In the present paper, we describe the results of an EPR investigation of four native defects that are formed during growth of a CSP crystal. These include cadmium, silicon, and phosphorus vacancies and silicon-on-cadmium antisites. The EPR spectrum from the singly ionized silicon vacancy (V_{Si}^{-}) is present at low temperature without exposure to laser light, whereas EPR signals from the singly ionized charge states of the cadmium vacancy (V_{Cd}^{-}) and the silicon-on-cadmium antisite (Si_{Cd}^{+}) and the neutral charge state of the

a)Author to whom correspondence should be addressed. Electronic mail: Larry.Halliburton@mail.wvu.edu.

phosphorus vacancy (V_P^0) must be photoinduced at low temperature using 632.8 nm light from a He-Ne laser. Identification of the defects is based on the resolved hyperfine patterns associated with neighboring ^{31}P nuclei. We report the g value, hyperfine spacings, and individual linewidths for each of the four defects when the magnetic field is along the [001] direction. In addition to these native defects, we observe EPR spectra[29,30] from Mn^{2+}, Fe^{+}, and Fe^{3+} ions that are unintentionally present. Our current investigation is an extension of earlier comprehensive identification studies[25,26,31–42] of native point defects in the closely related nonlinear chalcopyrite materials $ZnGeP_2$ and $ZnSiP_2$ (referred to as ZGP and ZSP). An initial brief survey of EPR and optical absorption spectra from Fe impurities and native defects in device-quality CSP crystals has been published.[43]

II. EXPERIMENTAL DETAILS

The undoped CSP single crystals used in the present study were grown at BAE Systems (Nashua, NH) using the horizontal gradient freeze method.[1] Samples with approximate dimensions of $3 \times 3 \times 5\,mm^3$ were cut from larger x-ray-oriented boules. All the data presented in this paper were obtained from one CSP crystal. In addition to the native defects, trace amounts of Mn^{2+} and Fe^{+} ions at Cd^{2+} sites and Fe^{3+} ions at Si^{4+} sites were observed in this sample (laser light produced the Fe^{+} and Fe^{3+} spectra but did not affect the Mn^{2+} spectrum). Crystals cut from other CSP boules grown at BAE Systems showed the same EPR spectra from the native defects and inadvertent impurities, but significant variations in the relative concentrations of these paramagnetic species were observed among the samples.[43] Neutral phosphorus-on-silicon antisite donors (P_{Si}^0) were not observed in our CSP samples,[44] just as neutral phosphorus-on-germanium antisites were not observed in ZGP crystals also grown by the horizontal gradient freeze method.[35]

The EPR spectra were taken with a Bruker EMX spectrometer operating near 9.40 GHz. An Oxford helium-gas flow system controlled the sample temperature, and a Bruker proton NMR teslameter measured the static magnetic field. A Cr-doped MgO crystal (Cr^{3+} ions have a known isotropic g value of 1.9800) was used to correct for small differences in magnetic field strength between the position of the sample and the tip of the teslameter probe. The CSP samples were illuminated at low temperature in the microwave cavity with 632.8 nm (1.96 eV) light from a He-Ne laser. The wavelength of these incident photons falls within the broad near-band-edge defect-related optical absorption bands observed in some, but not all, CSP crystals.[1]

III. CRYSTAL STRUCTURE

The CSP crystals are tetragonal with space group $I\bar{4}2d$ and belong to the large family of II-IV-V_2 chalcopyrite materials. These chalcopyrite structures can be generated from the III-V zincblende structure by replacing in an ordered manner half the group III ions with group II ions and half with group IV ions. A general view of the chalcopyrite crystal structure is shown in Fig. 1. The unique axis is the [001] direction (or c axis), and the two equivalent axes in the basal plane are the [100] and [010] directions (or a axes). Each cadmium ion is tetrahedrally bonded to four phosphorus ions, each silicon ion is also tetrahedrally bonded to four phosphorus ions, and each phosphorus has two cadmium and two silicon neighbors. The CSP lattice parameters,[45] at room temperature, are $a = 5.680$ Å, $c = 10.431$ Å, and $u = 0.2967$. The c/a ratio of 1.836 deviates considerably from 2.0 and indicates significant compression of the lattice along the [001] direction. Positions of the ions in the II-IV-V_2 chalcopyrite structure can be generated using the following minimum set of (x,y,z) coordinates (in units of the a and c constants):[46]

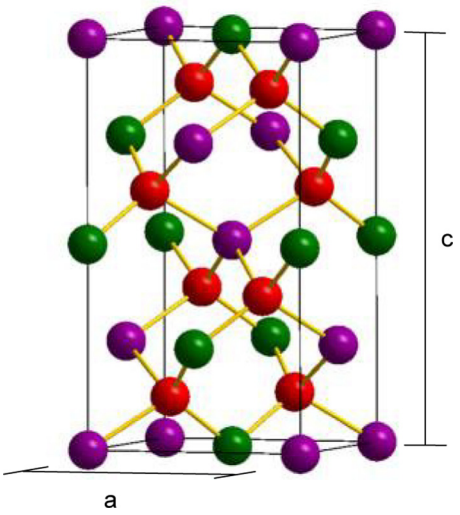

FIG. 1. Ball-and-stick representation of the $CdSiP_2$ crystal, a II-IV-V_2 chalcopyrite structure. The cadmium ions are purple, the silicon ions are green, and the phosphorus ions are red.

$$\text{Group II:}\quad (0,0,0),\ \left(0,\frac{1}{2},\frac{1}{4}\right),$$

$$\text{Group IV:}\quad \left(0,0,\frac{1}{2}\right),\ \left(0,\frac{1}{2},\frac{3}{4}\right),$$

$$\text{Group V:}\quad \left(u,\frac{1}{4},\frac{1}{8}\right),\ \left(-u,\frac{3}{4},\frac{1}{8}\right),\ \left(\frac{3}{4},u,\frac{7}{8}\right),\ \left(\frac{1}{4},-u,\frac{7}{8}\right).$$

The u parameter (when compared to 1/4) is a measure of the small "rotations" of the four anions surrounding each cation.[47] Rotations of these tetragonally distorted phosphorus tetrahedra about the c axis are caused by the different sizes of the cadmium and silicon ions. For fourfold coordination, the radius of Cd^{2+} ions is near 0.78 Å while the radius of Si^{4+} ions is only 0.26 Å.[48] Thus, a phosphorus ion shifts along an a axis toward its two silicon neighbors and away from its two cadmium neighbors, because the Cd-P bond lengths are greater than the Si-P bond lengths. This shifting in position of the four phosphorus ions about a cadmium ion in CSP is illustrated in Fig. 2. Interatomic distances and bond angles for the CdP_4 and SiP_4 tetrahedra in CSP are listed in Table I, along with the equivalent values for ZGP.[49] In CSP, the SiP_4 units retain the nearly perfect tetrahedron shape, whereas the CdP_4 units are significantly distorted tetrahedra. As seen in Table I, the "cation size effect" is less in

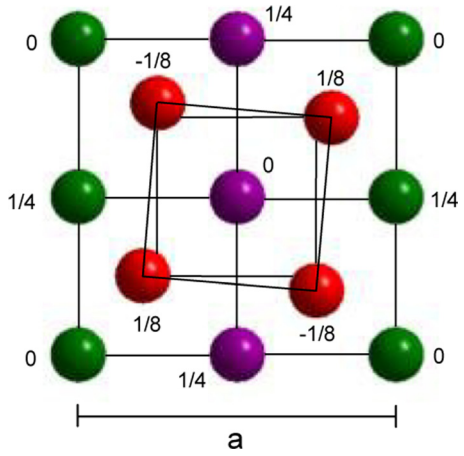

FIG. 2. A projection of the $CdSiP_2$ crystal on the [001] plane, illustrating the shifts of the four phosphorus ions around a cadmium ion. The numbers next to the ions are their z coordinates (in units of the c lattice constant) and the color scheme is the same as in Fig. 1.

ZGP. Although the small rotations of the CdP_4 and SiP_4 units about the c axis may be contributing factors, the most important structural feature that determines specific models for the native defects in CSP is the large difference in the Cd-P and Si-P bond lengths.

IV. EPR RESULTS

The EPR spectra from four distinct native defects in $CdSiP_2$ are individually described in this section. Each spectrum represents a defect with $S = 1/2$, and three of the four spectra have resolved hyperfine structure from ^{31}P nuclei. For these paramagnetic defects, the principal values of the g matrix do not deviate significantly from the free spin value of 2.0023, individual linewidths are relatively large, hyperfine splittings are not well resolved, and spectral lines from different defects strongly overlap in some cases. Thus, although attempts were made, it proved impossible to obtain angular dependence data that would allow unambiguous identification of site splittings for any of the defects. For these reasons, spectral characteristics are only reported for data taken with the magnetic field along the [001] direction in the crystal. All orientations, or sites, of a defect are degenerate (i.e., magnetically equivalent) for this direction and the simplest, and most informative, spectra are obtained. In every case, a defect model is firmly established by combining the information acquired from these [001] spectra with results from earlier studies of defects in $ZnGeP_2$. The following spin Hamiltonian with electron Zeeman and hyperfine terms describes our [001] EPR spectra:

$$H = g_c \beta S_z B + \sum_i A_{i,c} I_{i,z} S_z. \quad (1)$$

The index i will be 2 or 4, depending on the number of ^{31}P nuclei contributing to a resolved hyperfine pattern. (The last term is not needed if there is no resolved hyperfine.) Table II provides a comparison of the g_c and A_c parameters for native defects in $CdSiP_2$ and $ZnGeP_2$ crystals.

A. Silicon vacancy (V_{Si}^-)

Figure 3 shows the EPR spectrum from the singly ionized silicon vacancy (V_{Si}^-) in our CSP crystal. These data were obtained at 40 K with the magnetic field along the [001] direction. The sample was cooled in the dark and was not exposed to light while at 40 K. This spectrum consists of five equally spaced hyperfine lines having systematically varying intensities. Its g_c value is 2.0086, the hyperfine parameter A_c (i.e., the spacing between adjacent lines) is 4.01 mT, and the width of the individual lines is 1.6 mT. The spectrum has little angular dependence and is best observed near 40 K. At lower temperatures (<15 K), this spectrum is severely microwave-power saturated and thus is weak and distorted. The lines broaden at higher temperatures and the EPR signal is reduced in intensity, and the hyperfine structure is less resolved. Smaller EPR lines from trace amounts

TABLE I. Interatomic distances (in units of Å) and bond angles for the AP_4 and BP_4 tetrahedra in the ABP_2 chalcopyrite crystals, $CdSiP_2$ and $ZnGeP_2$. The multiplicity factor refers to the number of occurrences. These results were obtained from Refs. 45 and 49.

Distance or angle	Multiplicity	$CdSiP_2$	$ZnGeP_2$
AP_4 tetrahedra (A is Cd or Zn)			
A-P	4	2.561	2.375
P-P	4	4.064	3.856
P-P	2	4.407	3.924
∠P-A-P	4	105.0°	108.5°
∠P-A-P	2	118.8°	111.4°
BP_4 tetrahedra (B is Si or Ge)			
B-P	4	2.247	2.324
P-P	4	3.674	3.792
P-P	2	3.661	3.798
∠P-B-P	4	109.7°	109.3°
∠P-B-P	2	109.1°	109.6°

TABLE II. A comparison of spin-Hamiltonian parameters for native defects in $CdSiP_2$ and $ZnGeP_2$ crystals. The g value (g_c), the spacing between adjacent ^{31}P hyperfine lines (A_c), and linewidths (ΔB) are provided for three vacancy centers and one antisite in each material. These parameters were obtained from EPR spectra taken with the magnetic field along the [001] direction. Results for $CdSiP_2$ are from the present paper whereas results for $ZnGeP_2$ are from Refs. 31, 34, 35, and 37.

$CdSiP_2$	$ZnGeP_2$
Silicon vacancy (V_{Si}^-)	Germanium vacancy (V_{Ge}^-)
$g_c = 2.0086$	$g_c = 2.0123$
$A_c = 4.01$ mT	$A_c = 3.80$ mT
$\Delta B = 1.6$ mT	$\Delta B = 1.5$ mT
Cadmium vacancy (V_{Cd}^-)	Zinc vacancy (V_{Zn}^-)
$g_c = 2.0242$	$g_c = 2.038$
$A_c = 4.88$ mT	$A_c = 4.25$ mT
$\Delta B = 2.2$ mT	$\Delta B = 2.0$ mT
Phosphorus vacancy (V_P^0)	Phosphorus vacancy (V_P^0)
$g_c = 2.007$	$g_c = 2.079$
$\Delta B = 2.2$ mT	$\Delta B = 3.0$ mT
Silicon-on-cadmium antisite (Si_{Cd}^+)	Germanium-on-zinc antisite (Ge_{Zn}^+)
$g_c = 2.0060$	$g_c = 2.0026$
$A_c = 19.8$ mT	$A_c = 18.9$ mT
$\Delta B = 4.0$ mT	$\Delta B = 7.0$ mT

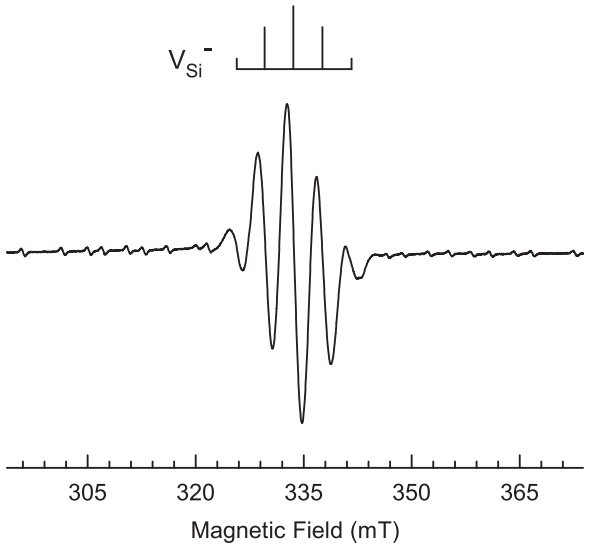

FIG. 3. Five-line EPR spectrum from the singly ionized silicon vacancy in $CdSiP_2$. These data were taken at 40 K with the magnetic field along the [001] direction and a microwave frequency of 9.381 GHz. This spectrum was not photoinduced (i.e., it was seen without exposure to laser light at low temperature). Weak lines from Mn^{2+} ions ($S = 5/2$, $I = 5/2$) are present above and below the silicon-vacancy spectrum.

of Mn^{2+} ions are seen in Fig. 3 in the magnetic field regions above and below the primary lines. These Mn^{2+} signals are not photoactive and are seen in all of the CSP samples.

The five-line spectrum in Fig. 3 has the characteristic appearance of an $S = 1/2$ unpaired electron interacting equally with four 100% abundant $I = 1/2$ nuclei. A spin system of this type gives five equally spaced hyperfine lines having relative intensities 1:4:6:4:1 with the separation between adjacent lines representing the magnitude of the hyperfine interaction with one of the four nuclei. Observed intensities in Fig. 3 are in good agreement with these predicted 1:4:6:4:1 ratios. The ^{31}P isotope is 100% abundant with $I = 1/2$ nuclear spin, and all of the cation sites in CSP have four ^{31}P nuclei as nearest neighbors. This means that the responsible defect must be at a cation site in the crystal, with the silicon vacancy being the most likely candidate because of the shorter Si-P bond lengths. There are also four phosphorus neighbors around both the cadmium vacancy and the silicon-on-cadmium antisite in CSP, but other EPR spectra are attributed to these defects in Sections IV B and IV D. As a result, the five-line EPR spectrum in Fig. 3 is assigned to singly ionized silicon vacancies in CSP. The model of this silicon-vacancy defect is illustrated in Fig. 4. Nearly equal and small P-P separation distances in the SiP_4 tetrahedron (see Table I) allow the unpaired electron to be equally shared by all four neighboring phosphorus ions. The analogous defect, the singly ionized germanium vacancy (V_{Ge}^-,) with five ^{31}P hyperfine lines in its EPR spectrum, has been observed during illumination of an electron-irradiated ZGP crystal.[37] Unlike the germanium vacancy in ZGP, the silicon vacancies we observe in CSP are formed during the growth of the crystal (i.e., the knock-on damage process associated with high-energy particle irradiations is not required to produce the silicon vacancy).

The three possible charge states of the silicon-vacancy acceptor are neutral (V_{Si}^0), singly ionized (V_{Si}^-), or doubly

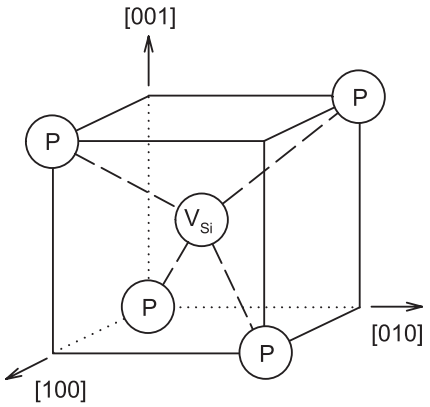

FIG. 4. The silicon vacancy in $CdSiP_2$ crystals has four nearest-neighbor phosphorus ions. In its singly ionized charge state, the unpaired electron is equally shared by these four neighbors. (All six P-P separation distances are nearly equal.) Small shifts in the phosphorus positions due to the different cation sizes are not included.

ionized ($V_{Si}^=$). Only the V_{Si}^- singly ionized charge state is paramagnetic. This EPR-active charge state of the silicon vacancy is present without light in our CSP samples, thus demonstrating that the crystals are compensated. The Fermi level is below the −/= level and above the 0/− level of the silicon vacancy. Other CSP crystals, with different concentrations of native defects and possibly large concentrations of impurities such as Fe, may not show the EPR spectrum from the singly ionized silicon vacancy unless they are exposed to near-band-edge light at liquid-helium temperatures.

B. Cadmium vacancy (V_{Cd}^-)

Figure 5 shows the EPR spectrum from the singly ionized cadmium vacancy (V_{Cd}^-) in our CSP crystal. These data were obtained at 6 K while exposing the crystal to 632.8 nm laser light. The magnetic field was along the [001] direction.

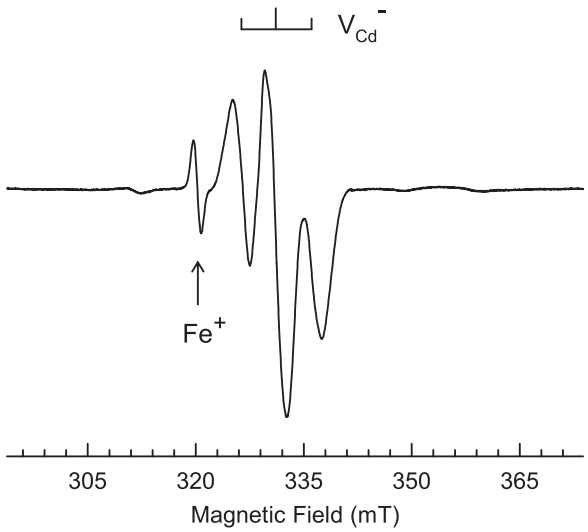

FIG. 5. Three-line EPR spectrum from the singly ionized cadmium vacancy in $CdSiP_2$. These data were taken at 6 K with the magnetic field along the [001] direction and a microwave frequency of 9.381 GHz. The sample was exposed to 632.8 nm laser light while the spectrum was being acquired. A single line from Fe^+ ions is seen at 320.0 mT.

Before illumination, this EPR signal was not seen in any of our CSP crystals. However, during illuminations at 6 K, the signal was present in all of the samples and always represented a large concentration of the defect. The EPR spectrum in Fig. 5 has three equally spaced hyperfine lines with relative intensities of 1:2:1. Its g_c value is 2.0242, the hyperfine parameter A_c (i.e., the spacing between adjacent lines) is 4.88 mT, and the width of the individual lines is 2.2 mT. This spectrum has only a small angular dependence and is best observed near 6 K. After removing the laser light, the three-line EPR spectrum disappears in a few seconds even though the sample remains at 6 K.[43] The EPR line at lower field in Fig. 5, with a g_c value of 2.0945, is due to Fe^{+} ($3d^7$) ions substituting for Cd^{2+} ions.[30]

The three-line spectrum in Fig. 5 is due to an $S = 1/2$ unpaired electron interacting equally with two 100% abundant $I = 1/2$ nuclei, which for this material must be ^{31}P nuclei. This produces three equally spaced hyperfine lines having relative intensities 1:2:1 with the separation between adjacent lines representing the magnitude of the hyperfine interaction with one of the two nuclei. The intensities in Fig. 5 are in good agreement with these predicted 1:2:1 ratios. Singly ionized zinc vacancies with a nearly identical three-line EPR hyperfine pattern have been observed in ZGP and ZSP crystals.[31–33,36–39] Because of its strong similarity with the zinc-vacancy spectra in ZGP and ZSP, the three-line EPR spectrum in Fig. 5 is assigned to the singly ionized cadmium vacancies in CSP.

The most striking features of the ground-state EPR spectra from the singly ionized zinc and cadmium vacancies in these chalcopyrite materials are the large hyperfine interactions with only two of the phosphorus neighbors, instead of all four of the phosphorus ions surrounding the vacancy. This primary sharing of the unpaired spin with just two of the phosphorus ions is caused by the large intrinsic distortion of the ZnP_4 and CdP_4 tetrahedra. Figure 6 illustrates the cadmium vacancy and its four phosphorus neighbors in CSP. As reported in Table I, the compression of the lattice along the [001] direction separates the six P-P distances in the CdP_4 unit into two sets. The P_1-P_3 and P_2-P_4 interatomic distances in Fig. 6 are 4.407 Å, while the remaining four interatomic distances (P_1-P_2, P_2-P_3, P_3-P_4, and P_4-P_1) are 4.064 Å. In ZGP and ZSP, the earlier EPR studies[31–33,39] verified that the unpaired electron at the zinc vacancy is localized on one of the pairs of phosphorus ions having the shorter interatomic spacing. This same behavior occurs for the singly ionized cadmium vacancies in the CSP crystals (as an example, the unpaired spin in Fig. 6 interacts equally with the ^{31}P nuclei at the P_1 and P_2 sites). Significant lattice relaxation may also be a contributing factor that helps localize the unpaired spin on only two phosphorus ions.

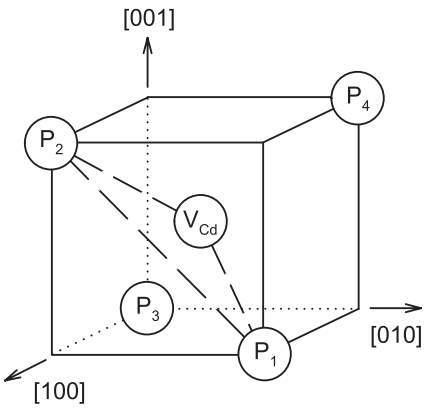

FIG. 6. The cadmium vacancy in $CdSiP_2$ crystals has four nearest-neighbor phosphorus ions. In its singly ionized charge state, the defect has the unpaired electron equally shared by the P_1 and P_2 neighbors. Other equivalent orientations of the defect have the unpaired spin shared by the P_2-P_3, P_3-P_4, and P_1-P_4 pairs of phosphorus ions. This model is simplified, in that it does not include the small shifts in the phosphorus positions due to the different cation sizes.

Similar to the silicon vacancy in CSP, the three possible charge states of the cadmium-vacancy acceptor are neutral (V_{Cd}^{0}), singly ionized (V_{Cd}^{-}), or doubly ionized ($V_{Cd}^{=}$). Only the V_{Cd}^{-} singly ionized charge state is paramagnetic. In both ZGP and ZSP, EPR signals from V_{Zn}^{-} centers are seen without photoexcitation. The EPR-active charge state of the cadmium vacancy, however, is only seen in our CSP samples during and immediately after exposure at very low temperature to 632.8 nm laser light. This means that the Fermi level in the as-grown CSP crystals is above the −/= acceptor level of the cadmium vacancy. Before the exposure to the laser light, the cadmium vacancy is in its doubly ionized charge state ($V_{Cd}^{=}$). The 632.8 nm light moves an electron to a donor or a deeper acceptor and allows the paramagnetic singly ionized state of the vacancy (V_{Cd}^{-}) to be observed. A primary mechanism causing the rapid disappearance at 6 K of the V_{Cd}^{-} center EPR spectrum when the light is removed has not been established. Electrons released from the neutral donors described in Section IV C could be responsible for this decay (i.e., these donors may act as short-lived electron traps). Or it is possible that the doubly ionized state of the silicon vacancy ($V_{Si}^{=}$) is populated by the light at 6 K and then rapidly loses the electron when the light is turned off. When compared to the zinc vacancy in ZGP, the larger P-P separations in the CdP_4 tetrahedra (see Table I) may be a significant factor in causing the shallow nature of the cadmium vacancy in CSP.

C. Phosphorus vacancy (V_P^0)

Direct evidence for the presence of phosphorus vacancies in our CSP crystals is obtained by comparing light-off and light-on EPR spectra. The five-line spectrum from the singly ionized silicon vacancy (V_{Si}^{-}) taken before exposure to 632.8 nm laser light is shown in Fig. 7(a). (This is the same as the spectrum in Fig. 3.) These data were acquired at 40 K with the field along the [001] direction. The EPR spectrum in Fig. 7(b) was then taken from the same sample during an exposure to 632.8 nm light. The spectrometer settings and the sample temperature are the same in Figs. 7(a) and 7(b). Comparing the intensities in Figs. 7(a) and 7(b) of the two highest-field V_{Si}^{-} lines (at 337.7 and 341.8 mT) shows that the near-band-edge light reduced the concentration of V_{Si}^{-} acceptors. At the same time, spectra from two intrinsic donors (the neutral phosphorus vacancy and the singly ionized silicon-on cadmium antisite) and Fe^{3+} impurities appear

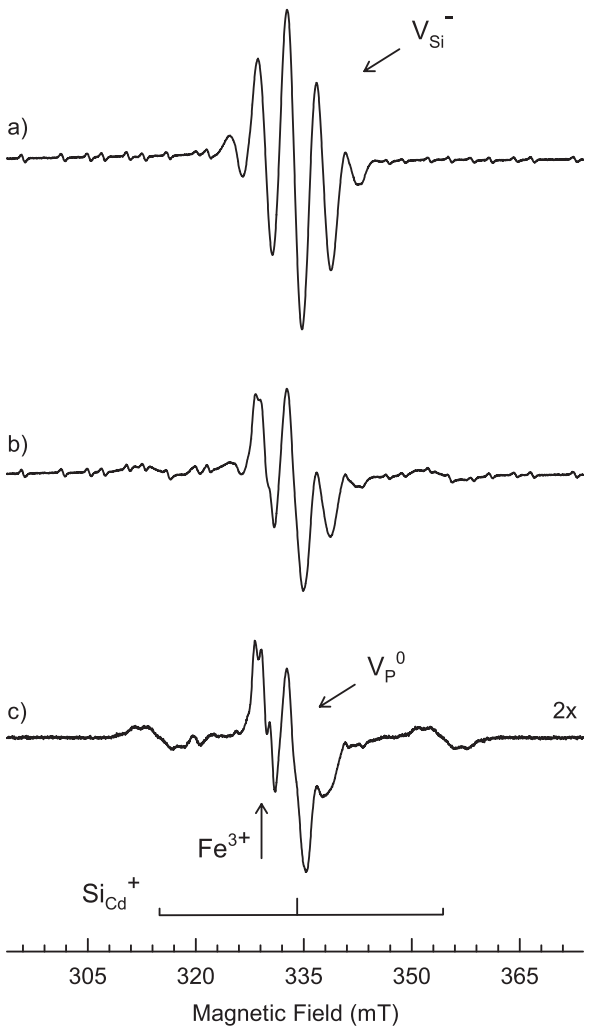

FIG. 7. A comparison of EPR spectra from $CdSiP_2$ taken at 40 K with the magnetic field along the [001] direction and a microwave frequency of 9.381 GHz. (a) Spectrum taken without light, showing the signals from the five-line silicon vacancy. (b) Spectrum taken under identical conditions, except now the crystal is exposed to 632.8 nm laser light. (c) Difference spectrum after eliminating the Mn^{2+} and V_{Si}^- spectra (the intensity of this spectrum has been increased by a factor of two). The signals in spectrum (c) are from the phosphorus vacancy (V_P^0), the silicon-on-cadmium antisite (Si_{Cd}^+), and an impurity (Fe^{3+}).

in Fig. 7(b) along with the smaller V_{Si}^- spectrum. The signals from these additional defects, however, are strongly overlapping in Fig. 7(b) and thus are not readily distinguished.

These three new photoinduced EPR spectra are more easily seen in Fig. 7(c). Two steps were involved in extracting the individual signals in Fig. 7(c) from the spectra in Figs. 7(a) and 7(b). Weak Mn^{2+} EPR lines in the low and high field regions in Figs. 7(a) and 7(b) have the same intensities (i.e., they are not affected by the laser light), and thus a subtraction eliminates them from Fig. 7(c). Next, the intensity of the V_{Si}^- spectrum in Fig. 7(a) was multiplied by a factor of 0.67 to account for its photoinduced decrease, and the result was then subtracted from Fig. 7(b) in order to eliminate the V_{Si}^- spectrum from Fig. 7(c). This procedure effectively leaves in Fig. 7(c) the spectra of the three paramagnetic trapped-electron defects that are populated when electrons are moved by the light from singly ionized silicon vacancies (V_{Si}^-) to the higher lying electron-trapping states. To better illustrate these three EPR spectra, the intensity of the spectrum in Fig. 7(c) has been increased by a factor of 2. The neutral phosphorus vacancy (V_P^0) is the single line near 333.9 mT, the structured signal near 329.3 mT (with $g_c = 2.036$ and ^{31}P hyperfine spacings of ~1.3 mT) is assigned to Fe^{3+} ions ($S = 5/2$) replacing Si^{4+} ions,[30] and the silicon-on-cadmium antisite (described in detail in Section IV D) has a widely split three-line spectrum identified by the stick diagram below the spectrum in Fig. 7(c). All three photoinduced electron-trapping centers in Fig. 7(c) thermally decay when the light is removed while the sample remains at 40 K. The V_P^0 and Fe^{3+} signals disappear within a few minutes in the dark while the Si_{Cd}^+ signal decays much slower, on the order of tens to hundreds of minutes. The V_{Si}^- spectrum also returns very slowly at 40 K to its pre-illumination intensity (at a rate similar to the decay of the Si_{Cd}^+ signal).

The photoinduced EPR spectrum from the neutral phosphorus vacancy (V_P^0) near 333.9 mT in Fig. 7(c) has a linewidth of approximately 2.2 mT and has no resolved hyperfine structure from nearby ^{31}P nuclei. Because of strong overlap of lines in Fig. 7(b), no attempt was made to determine the angular dependence of the V_P^0 spectrum. The g_c value of the phosphorus vacancy in CSP is 2.007. In contrast, the g_c value for the neutral phosphorus vacancy in ZGP is 2.079.[34] This much smaller g shift in CSP (from the free-spin value of 2.0023) strongly suggests that the unpaired spin associated with this defect is primarily localized on one or both of the adjacent silicon ions. These g shifts for V_P^0 in ZGP and CSP are caused by spin-orbit interactions and are different in the two materials because the spin-orbit coupling constants of silicon and germanium are significantly different (λ_{Ge} is 940 cm^{-1} whereas λ_{Si} is 142 cm^{-1}).[50] If the unpaired spin were localized on group II neighbors in CSP and ZGP, then the g shift for the neutral phosphorus vacancy would be greater in CSP than ZGP because cadmium has a larger spin-orbit coupling constant than zinc. This latter prediction is the opposite of the experimental observation, and thus provides additional verification that the unpaired spin is, to a large extent, on group IV ions adjacent to the phosphorus vacancy. A theoretical study[41] of the neutral phosphorus vacancy in ZGP has also suggested that the defect's unpaired spin is localized on the adjacent germanium neighbors. Figure 8 shows the model of the neutral phosphorus vacancy in CSP.

D. Silicon-on-cadmium antisite (Si_{Cd}^+)

Figure 7(c) includes the photoinduced EPR spectrum from the singly ionized silicon-on-cadmium antisite (Si_{Cd}^+) in CSP. These data were obtained at 40 K with the magnetic field along the [001] direction. This spectrum consists of three broad and equally spaced hyperfine lines having 1:2:1 ratios that are due to hyperfine interactions with two ^{31}P nuclei. Overlap with the large phosphorus-vacancy (V_P^0) signal obscures much of the middle broad line, but its high-field side is seen near 338.0 mT. The Si_{Cd}^+ center has a g_c value of 2.0060, its A_c hyperfine parameter (i.e., the spacing between adjacent lines) is 19.8 mT, and the width of the individual

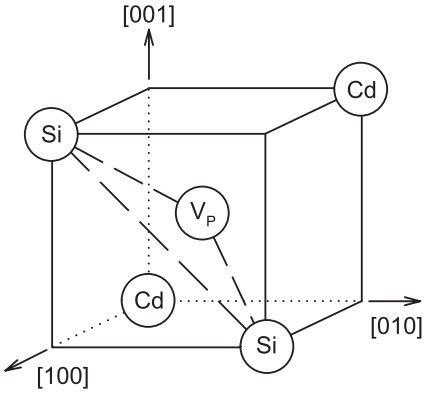

FIG. 8. The phosphorus vacancy in $CdSiP_2$ has two silicon and two cadmium neighbors. In its neutral charge state, the defect has the unpaired electron localized primarily on one or both of the silicon neighbors. This model is also simplified, in that it does not include the small shift in the phosphorus ion position due to the different cation sizes.

lines is 4.0 mT. The spectrum has very little angular dependence. An EPR spectrum from the germanium-on-zinc (Ge^{+}_{Zn}) antisite has been previously reported in ZGP crystals.[35] This spectrum in ZGP has the same widely split three-line hyperfine pattern as CSP. When the magnetic field is along the [001] direction, the adjacent lines are 18.9 mT apart in ZGP and g_c is 2.0026.

In CSP, the silicon ions are much smaller than the cadmium ions (see Section III). When the silicon ion replaces the cadmium ion, this difference in size allows the silicon ion to move off-center and assume an equilibrium position that is closer to two of its phosphorus neighbors, thus explaining the experimental observation that the unpaired spin has a large hyperfine interaction with only two of the neighboring ^{31}P nuclei. This displacement could be along either of the two equivalent [100] directions or along the [001] direction. The lack of angular dependence data prevents us from establishing which type of displacement actually occurs (computational studies may resolve this question). For illustrative purposes, a model of the silicon-on-cadmium antisite corresponding to a displacement along a [100] direction is shown in Fig. 9.

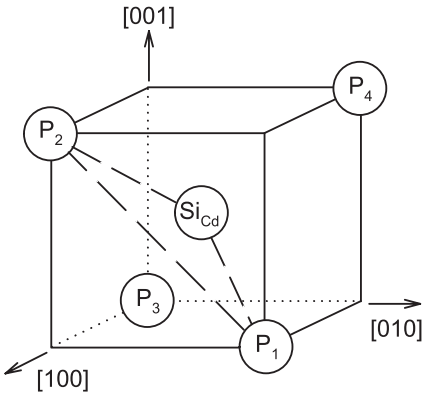

FIG. 9. The silicon-on-cadmium antisite in $CdSiP_2$ has four nearest-neighbor phosphorus ions. In its singly ionized charge state, the defect has the unpaired electron equally shared by two of these phosphorus neighbors. Small shifts in the phosphorus positions due to the different cation sizes are not included in the model.

Before exposing the CSP crystal to the 632.8 nm laser light, this antisite donor is in the doubly ionized charge state (Si^{++}_{Cd}). Light then moves an electron from an acceptor to the antisite and forms the Si^{+}_{Cd} singly ionized donor. In the nonparamagnetic Si^{++}_{Cd} charge state, the four sp^3 hybrid bonds that the silicon ion makes with its phosphorus neighbors are each filled with two electrons (spin up and spin down). Thus, the additional electron that converts the doubly ionized Si^{++}_{Cd} antisite to the singly ionized Si^{+}_{Cd} donor will occupy a state with more s nature and less p nature. This latter behavior explains why there is very little angular dependence associated with the Si^{+}_{Cd} donor and why the magnitudes of the ^{31}P hyperfine interactions are larger for the Si^{+}_{Cd} donor than for the V^{-}_{Si} and V^{-}_{Cd} acceptors.

V. SUMMARY

EPR is used at low temperature to investigate native defects in $CdSiP_2$ crystals. These crystals are highly compensated (i.e., both donors and acceptors are present). Included in the study are silicon, cadmium, and phosphorus vacancies, along with silicon-on-cadmium antisites. In all cases except the silicon vacancies, a paramagnetic charge state of the defect must be photoinduced with 632.8 nm laser light at liquid helium temperatures. Ground-state models of the EPR-active defects are proposed that are consistent with the observed ^{31}P hyperfine interactions and the relative sizes of the Si and Cd ions. Future correlation studies involving EPR and optical absorption measurements will allow near and mid-infrared absorption bands to be assigned to specific native defects. This, in turn, will permit crystal-growth efforts to focus on eliminating defects that affect the performance of CSP-based optical parametric oscillators used to generate tunable mid-infrared laser light.

ACKNOWLEDGMENTS

Work at the Air Force Institute of Technology (EMG) was supported by the AFIT Faculty Research Initiation Program and work at BAE Systems (KTZ and PGS) was supported by the Air Force Research Laboratory (Wright-Patterson AFB) through Contract No. FA8650-05-C-5425. The views expressed in this paper are those of the authors and do not necessarily reflect the official policy or position of the Air Force, the Department of Defense, or the United States Government.

[1]K. T. Zawilski, P. G. Schunemann, T. C. Pollak, D. E. Zelmon, N. C. Fernelius, and F. K. Hopkins, J. Cryst. Growth **312**, 1127 (2010).
[2]V. Petrov, Prog. Quantum Electron. **42**, 1 (2015).
[3]Z. He, B. Zhou, S. Zhu, B. Chen, H. Hou, Y. Yu, and L. Xie, Comput. Mater. Sci. **72**, 26 (2013).
[4]Z. L. Lv, Y. Cheng, X. R. Chen, and G. F. Ji, Comput. Mater. Sci. **77**, 114 (2013).
[5]V. Kemlin, P. Brand, B. Boulanger, P. Segonds, P. G. Schunemann, K. T. Zawilski, B. Menaert, and J. Debray, Opt. Lett. **36**, 1800 (2011).
[6]V. Kemlin, B. Boulanger, V. Petrov, P. Segonds, B. Menaert, P. G. Schunemann, and K. T. Zawilski, Opt. Mater. Express **1**, 1292 (2011).
[7]L. Fan, S. Zhu, B. Zhao, B. Chen, Z. He, H. Yang, and G. Liu, J. Cryst. Growth **338**, 228 (2012).
[8]G. Zhang, X. Tao, H. Ruan, S. Wang, and Q. Shi, J. Cryst. Growth **340**, 197 (2012).

[9]L. Fan, S. Zhu, B. Zhao, B. Chen, Z. He, H. Yang, G. Liu, and X. Wang, J. Cryst. Growth **364**, 62 (2013).
[10]G. D. Zhang, H. P. Ruan, X. Zhang, S. P. Wang, and X. T. Tao, CrystEngComm **15**, 4255 (2013).
[11]V. Petrov, P. G. Schunemann, K. T. Zawilski, and T. M. Pollak, Opt. Lett. **34**, 2399 (2009).
[12]V. Petrov, G. Marchev, P. G. Schunemann, A. Tyazhev, K. T. Zawilski, and T. M. Pollak, Opt. Lett. **35**, 1230 (2010).
[13]O. Chalus, P. G. Schunemann, K. T. Zawilski, J. Biegert, and M. Ebrahim-Zadeh, Opt. Lett. **35**, 4142 (2010).
[14]S. C. Kumar, A. Agnesi, P. Dallocchio, F. Pirzio, G. Reali, K. T. Zawilski, P. G. Schunemann, and M. Ebrahim-Zadeh, Opt. Lett. **36**, 3236 (2011).
[15]G. Marchev, A. Tyazhev, V. Petrov, P. G. Schunemann, K. T. Zawilski, G. Stoeppler, and M. Eichhorn, Opt. Lett. **37**, 740 (2012).
[16]S. C. Kumar, M. Jelínek, M. Baudisch, K. T. Zawilski, P. G. Schunemann, V. Kubeček, J. Biegert, and M. Ebrahim-Zadeh, Opt. Express **20**, 15703 (2012).
[17]G. Marchev, F. Pirzio, R. Piccoli, A. Agnesi, G. Reali, P. G. Schunemann, K. T. Zawilski, A. Tyazhev, and V. Petrov, Opt. Lett. **37**, 3219 (2012).
[18]G. Marchev, F. Pirzio, A. Agnesi, G. Reali, V. Petrov, A. Tyazhev, P. G. Schunemann, and K. T. Zawilski, Opt. Commun. **291**, 326 (2013).
[19]A. Tyazhev, F. Pirzio, A. Agnesi, G. Reali, V. Petrov, G. Marchev, P. G. Schunemann, and K. T. Zawilski, Appl. Phys. B **112**, 453 (2013).
[20]N. Hendaoui, A. Peremans, P. G. Schunemann, K. T. Zawilski, and V. Petrov, Laser Phys. **23**, 085401 (2013).
[21]G. Marchev, F. Pirzio, R. Piccoli, A. Agnesi, G. Reali, P. G. Schunemann, K. T. Zawilski, A. Tyazhev, and V. Petrov, Opt. Lett. **38**, 3344 (2013).
[22]Z. W. Zhang, D. T. Reid, S. C. Kumar, M. Ebrahin-Zadeh, P. G. Schunemann, K. T. Zawilski, and C. R. Howle, Opt. Lett. **38**, 5110 (2013).
[23]S. C. Kumar, J. Krauth, A. Steinmann, K. T. Zawilski, P. G. Schunemann, H. Giessen, and M. Ebrahim-Zadeh, Opt. Lett. **40**, 1398 (2015).
[24]N. C. Giles and L. E. Halliburton, MRS Bull. **23**, 37 (1998).
[25]S. D. Setzler, P. G. Schunemann, T. M. Pollak, M. C. Ohmer, J. T. Goldstein, F. K. Hopkins, K. T. Stevens, L. E. Halliburton, and N. C. Giles, J. Appl. Phys. **86**, 6677 (1999).
[26]N. C. Giles, L. Bai, M. M. Chirila, N. Y. Garces, K. T. Stevens, P. G. Schunemann, S. D. Setzler, and T. M. Pollak, J. Appl. Phys. **93**, 8975 (2003).
[27]J. A. Weil and J. R. Bolton, *Electron Paramagnetic Resonance: Elementary Theory and Practical Applications*, 2nd ed. (John Wiley and Sons, New York, 2007).
[28]J.-M. Spaeth and H. Overhof, *Point Defects in Semiconductors and Insulators: Determination of Atomic and Electronic Structure from Paramagnetic Hyperfine Interactions*, Springer Series of Materials Science Vol. 51 (Springer, Berlin, 2003).
[29]U. Kaufmann, A. Räuber, and J. Schneider, Phys. Status Solidi B **74**, 169 (1976).
[30]U. Kaufmann, Phys. Rev. B **14**, 1848 (1976).
[31]M. H. Rakowsky, W. K, Kuhn, W. J. Lauderdale, L. E. Halliburton, G. J. Edwards, M. P. Scripsick, P. G. Schunemann, T. M. Pollak, M. C. Ohmer, and F. K. Hopkins, Appl. Phys. Lett. **64**, 1615 (1994).
[32]L. E. Halliburton, G. J. Edwards, M. P. Scripsick, M. H. Rakowsky, P. G. Schunemann, and T. M. Pollak, Appl. Phys. Lett. **66**, 2670 (1995).
[33]K. T. Stevens, S. D. Setzler, L. E. Halliburton, N. C. Fernelius, P. G. Schunemann, and T. M. Pollak, *Infrared Applications of Semiconductors II*, edited by D. L. McDaniel, Jr., M. O. Manasreh, R. H. Miles, and S. Sivananthan, Mater. Res. Soc. Symp. Proc. **484**, 549 (1998).
[34]N. C. Giles, L. E. Halliburton, P. G. Schunemann, and T. M. Pollak, Appl. Phys. Lett. **66**, 1758 (1995).
[35]S. D. Setzler, N. C. Giles, L. E. Halliburton, P. G. Schunemann, and T. M. Pollak, Appl. Phys. Lett. **74**, 1218 (1999).
[36]W. Gehlhoff, R. N. Pereira, D. Azamat, A. Hoffmann, and N. Dietz, Physica B **308–310**, 1015 (2001).
[37]W. Gehlhoff, D. Azamat, and A. Hoffmann, Phys. Status Solidi B **235**, 151 (2003).
[38]W. Gehlhoff, D. Azamat, and A. Hoffmann, Mater. Sci. Semicond. Process. **6**, 379 (2003).
[39]W. Gehlhoff, D. Azamat, A. Krtschil, A. Hoffmann, and A. Krost, Physica B **340–342**, 933 (2003).
[40]P. Zapol, R. Pandey, M. Ohmer, and J. Gale, J. Appl. Phys. **79**, 671 (1996).
[41]X. S. Jiang, M. S. Miao, and W. R. L. Lambrecht, Phys. Rev. B **73**, 193203 (2006).
[42]X. S. Jiang and W. R. L. Lambrecht, Solid State Commun. **149**, 685 (2009).
[43]N. C. Giles, L. E. Halliburton, S. Yang, X. Yang, A. T. Brant, N. C. Fernelius, P. G. Schunemann, and K. T. Zawilski, J. Cryst. Growth **312**, 1133 (2010).
[44]U. Kaufmann, J. Schneider, and A. Räuber, Appl. Phys. Lett. **29**, 312 (1976).
[45]S. C. Abrahams and J. L. Bernstein, J. Chem. Phys. **55**, 796 (1971).
[46]G. Burns and A. M. Glazer, *Space Groups for Solid State Scientists*, 2nd ed. (Academic Press, San Diego, 1990), p. 198.
[47]A. Continenza, S. Massidda, A. J. Freeman, T. M. de Pascale, F. Meloni, and M. Serra, Phys. Rev. B **46**, 10070 (1992).
[48]J. A. Van Vechten and J. C. Phillips, Phys. Rev. B **2**, 2160 (1970).
[49]M. D. Lind and R. W. Grant, J. Chem. Phys. **58**, 357 (1973).
[50]P. Somers, A. Stesmans, L. Souriau, and V. V. Afanas'ev, J. Appl. Phys. **112**, 074501 (2012).